



OPEN Sepsis insult generates different vascular response phenotypes: an unsupervised time-series clustering preclinical study

Imre Vida, Marta Carrara[✉] & Manuela Ferrario

In this study, the temporal evolution of the cardiovascular response to sepsis was investigated by combining conventional hemodynamic parameters with novel indices derived from arterial blood pressure (ABP) waveforms that reflect vascular properties. The well-established association between sepsis and vascular dysfunction suggests that waveform-based indices may be instrumental in sepsis early detection and quantitative assessment of sepsis severity. ABP was continuously recorded at aortic and femoral sites in 40 pigs from a baseline condition to the full development of septic shock which was induced by intraperitoneal instillation of autologous feces. Standard beat-to-beat indices, including mean ABP, heart rate, and pulse pressure (PP), were computed alongside advanced cardiovascular markers such as baroreflex sensitivity, characteristic time constant (τ), PP amplification, and harmonic distortion (HD). Time series clustering was performed using a K-mean clustering approach with soft-dynamic time warping distance metric using 4 features - PP amplification, femoral τ , aortic systolic ABP, and femoral HD - selected by the First Integer Neighbor Clustering Hierarchy filtering method. According to the main physiological parameters typically evaluated by clinicians, all animals experienced severe cardiovascular decompensation under septic conditions. However, the time series cluster analysis identified two clusters with distinct temporal patterns of the cardiovascular variables. Shapelet analysis confirmed these findings, revealing consistent variable-specific trends. The proposed indices may assist clinicians in the early identification of sepsis and monitoring of sepsis severity, supporting more timely and personalized therapeutic strategies. Further studies are needed to explore their relationship with treatment response and clinical outcomes.

Keywords Arterial blood pressure waveform, Sepsis, Time-series clustering, Vascular dysfunction, Cardiovascular response

Sepsis and septic shock remain among the leading causes of mortality in intensive care units (ICUs), accounting for nearly 20% of global deaths¹. Beyond the acute phase, many sepsis survivors face long-term consequences, including impairments in immune, cognitive, psychiatric, renal, and cardiovascular systems^{2,3}. Nearly one-quarter of these patients are readmitted within 30 days of discharge⁴, and the five-year mortality among survivors may reach up to 75%⁵. Furthermore, sepsis has recently been proposed as a long-term risk factor for cardiovascular disease, with relative risk levels comparable to traditional risk factors such as hypertension and diabetes mellitus⁶.

The pathophysiological changes associated with sepsis and septic shock are complex and progressive, significantly impacting the cardiovascular system. Key features include vasoplegia, disrupted microvascular flow, and widespread endothelial dysfunction. These alterations are typically heterogeneous across the vascular tree, leading to regional variations in vascular tone, pathological vasodilation, and impaired adrenergic responsiveness. Previous studies have reported stiffening of large vessels (e.g., the aorta) and, conversely, increased compliance and reduced resistance in peripheral vessels. This contributes to a phenomenon known as peripheral vascular decoupling—marked by a reversal of the physiological amplification of pulse pressure (PP) from central to peripheral arteries^{7,8}.

Department of Electronics, Information and Bioengineering, Politecnico di Milano, Milan, Italy. ✉email: marta.carrara@polimi.it

Currently, the diagnosis of septic shock relies primarily on clinical symptoms and laboratory findings, such as hypotension, fever, respiratory distress, and high level of lactate⁹. However, these signs are often only recognized after the condition has significantly progressed, when organ support is required, too late for an early, individualized intervention. There is a critical need to improve patient monitoring systems in the ICU to detect early signs of clinical deterioration and better stratify the risk of progression to septic shock.

While recent research has focused on using electronic health records (EHR) to develop machine learning models for the risk stratification, few studies have explored the potential of high-resolution physiological signals continuously monitored at the bedside. Signals such as invasive arterial blood pressure and electrocardiogram, routinely recorded in critically ill patients, contain valuable physiological information that remains largely underexploited^{10–12}. These signals can be used to extract advanced features that may offer early and sensitive markers of cardiovascular deterioration^{13–18}.

Our research group has observed significant heterogeneity in the timing and severity progression in animal experiments of septic shock induced by intraperitoneal instillation of autologous feces^{12,19}. The aim of this study was to investigate the cardiovascular response to sepsis over time, from the initial inflammatory response to the complete onset of septic shock. We monitored both standard hemodynamic parameters—mean arterial pressure (MAP), heart rate (HR), cardiac output (CO)—and novel arterial blood pressure waveform-derived indices that reflect vascular properties, including PP amplification, the Windkessel time constant (τ), and harmonic distortion (HD). The ultimate goal of this work is to assess whether the continuous monitoring of these novel waveform-derived markers can improve early detection and severity assessment of septic deterioration, potentially contributing to more timely and personalized treatment strategies in critically ill patients.

Methods

Experimental datasets

The data used for this study comes from various swine experiments designed to study different resuscitation strategies and therapies, but with similar protocol to induce septic shock.

52 pigs (*Sus scrofa domesticus*, RA-SE Genetics, Belgium, weight 45.8 ± 5.8 kg, male = 22(64.7%) referred to 34 animals out of 52) were collected in the following experiments: Ivabradine and Esmolol study ($n = 15$)¹², ShockOmics study ($n = 6$)⁸, Noradrenaline and Angiotensin-II study ($n = 16$)²⁰, Noradrenaline and Procizumab study ($n = 15$)²¹. All the experiments were conducted in the Experimental Laboratory of Intensive Care (LA1230336), at the Université Libre de Bruxelles with the approval of the local animal ethics committee (CEBEA ULB). The protocols followed the EU Directive (2010/63/ EU) for animal experiments, the ARRIVE guidelines, and MQTiPSS recommendations for translational research in sepsis^{22,23}.

Animals were fasted for 18 h prior to the start of the experiment with free access to water. Thereafter, they were sedated with an intramuscular injection of midazolam (1 mg/kg) and ketamine hydrochloride (20 mg/kg) in the neck for the Angiotensin-II and Procizumab studies, and with 1.5 mg/kg midazolam and 5 mg/kg azaperone for the ShockOmics and Ivabradine/Esmolol studies. Following anesthesia induction with an intravenous injection of 3 μ g/kg of sufentanyl, 1 mg/kg of propofol and 0.5 mg/kg of rocuronium, endotracheal intubation was performed. General anesthesia was achieved with continuous inhalation of sevoflurane (at 1.8 to 2.5% alveolar concentration) and analgesia with continuous infusion of morphine (0.2–0.5 mg/kg/h, the optimal dose being determined through repeated pain tests, i.e., change in heart rate or blood pressure after nasal septum pinching), in association with rocuronium (1.8 to 2.0 mg/kg/h). In the ShockOmics and Ivabradine/Esmolol studies sufentanil (1–4 μ g/kg/h) was used instead of morphine.

After anesthesia and instrumentation with a closed-chest, minimally invasive approach, the animals were allowed to rest and stabilize for approximately two hours before baseline measurements were recorded. Sepsis was then induced by intraperitoneal instillation of 3 g/kg of autologous feces—filtered and diluted in 300 ml of 5% glucose solution—administered through two abdominal drains. From the onset of sepsis, a balanced crystalloid solution (Plasmalyte, Baxter, Belgium) was administered as the sole maintenance fluid at a low rate of 1 ml/kg/h. Once the animals developed hypotension, defined as a MAP below 50 mmHg, the infusion rate was modestly increased to maintain MAP within the 45–50 mmHg range for an additional hour. This phase aimed to consolidate the peripheral hypoperfusion and the onset of multiple organ failure. At the end of this period, a second time point was defined as reference for non-resuscitated septic shock condition. The animals were then resuscitated using either standard therapy or with the adjunction of non-traditional drugs, depending on the protocol. However, this part of the protocols is not relevant for the present study, which focuses solely on the septic shock development, i.e. before the clinical manifestation of sepsis and its resuscitation. After completion of the experiment, the animals were euthanized with 40 mL of 7.5% potassium chloride injection under deep anesthesia and the adjunction of an overdose of thiopental in the Ivabradine/Esmolol and Shockomics studies. The analyses were performed in this study from the baseline, i.e., few minutes before the feces inoculation, until the septic shock development; thus, the different resuscitation strategies and their impact on the outcome were not investigated as they does not affect the overall findings of the present study.

Aortic, femoral, and radial arterial blood pressure (ABP) were continuously measured at 500–250 Hz using high-fidelity pressure solid tip transducer catheters for aortic and femoral signals, and a fluid filled catheter with an external transducer for radial blood pressure. Continuous CO monitoring was performed using a pulmonary artery catheter (CCO; Edwards LifeSciences, Irvine, CA, United States) and recorded at 250 Hz. Each signal was exported to an A/D recording station (Notocord Hem, Notocord, France).

Ten animals were excluded due to missing femoral recordings, 1 due to missing CO values, and 1 due to too noisy recordings. A total of 40 pigs were considered for successive analyses.

Preprocessing and parameters extraction

The following analyses were performed in the Matlab framework (MathWorks). All the signals were firstly resampled at 125 Hz. Beat-to-beat time series of systolic (SAP), diastolic (DAP) pressures, MAP, and PP, computed as the difference between SAP and DAP values within the same beat, were obtained from the ABP waveforms using standard algorithms^{24,25}. The time series of heart period (HP) was obtained from the aortic ABP waveform by computing the time difference between two consecutive onsets of ABP beats and considered as a surrogate of the RR-intervals time series. Beat-to-beat HR was computed as 60/HP [bpm]. All onset points were visually checked and missed onsets were manually placed. A quality check of the signals was performed manually by visual inspection and noisy regions were defined as segments in which the morphology of ABP signal was unrecognizable or corrupted by artefacts like saturation or high frequency noise; the noisy regions were manually flagged to be excluded from subsequent analyses.

Stroke volume (SV) was calculated as CO/HR. Arterial compliance (AC) was determined by dividing SV by PP. Total peripheral resistance (TPR) was computed as MAP/CO. Diastolic shock index (DSI) and systolic shock index (SSI) were calculated as HR/DAP and HR/SAP, respectively²⁶. PP amplification was computed as the ratio between femoral or radial PP and aortic PP.

The computed indices were subdivided into consecutive 2-minute intervals and averaged within the window to obtain 2-minute time series for each index.

For each 2-minute segment of ABP waveform, other composite cardiovascular indices were computed:

- i) *Cardiac baroreflex sensitivity (BRS)*. Cardiac baroreflex is the most important short-term feedback mechanism responsible for ABP regulation, and it is mediated by the autonomic nervous system. It can be quantified by the evaluation of BRS. In this work, BRS was estimated by adopting the bivariate closed-loop model method on the time series of SAP and HP, firstly resampled at 2 Hz²⁷. The evaluation of cardiac BRS was limited to the low-frequency (LF, 0.04–0.15 Hz) component only, as this component carries information about sympathetic activity; moreover, the high-frequency component lacks physiological interpretability, as it is entirely driven by the mechanical ventilator.
- ii) *Feedforward gain (FF)*. We also computed the FF gain through the same model adopted for BRS²⁷, to estimate the influence of HP variability on SAP variability due to the mechanical coupling between the cardiac and the vascular system. This gain was computed in the LF band only.
- iii) *ABP waveform Harmonic Distortion*. HD index was estimated on a waveform template computed within each 2-minute time window of the ABP signal²⁸. The following criteria were used to ensure that outliers and ectopic beats were not included in the computation of the ABP beat template: we only considered the ABP beats that had a duration differing by no more than ± 80 ms, PP values within ± 3 , where is the standard deviation of the 2-minute ABP signal, and a systolic peak location differing no more than ± 80 ms. The ABP beat template was then created by averaging the selected beats, and aligning them based on their onsets. Finally, HD index was computed on each ABP template as:

$$HD = \frac{\sum_{k=2}^6 ABP_k}{ABP_1} \quad (1)$$

where ABP_k is the k -th coefficient of the Fourier Series computed on ABP template.

- iv) *The Windkessel time constant τ* . It is defined as the product of TPR and AC, $\tau = AC \bullet TPR$, and describes the exponential decay of the ABP pulse from the systolic peak to the end of diastole²⁹. To obtain a robust estimate, we adopted the method proposed by Mukkamala and colleagues³⁰, which estimates the exponential decay over 6-minute windows by adopting a black-box model approach. This method avoids the cumulative effects of wave reflections, which are attenuated in the central ABP waveforms only. More specifically, the ABP response to a single, solitary cardiac contraction is estimated from the 6-minute ABP segment. Then, the Windkessel time constant is measured by fitting an exponential curve to the estimated response after the initial peak, when the contribution of faster wave reflections is supposed to have disappeared. The τ calculation has been computed on 6-minute long ABP segments shifted every 2 min.

At the end of this process, we obtained a set of cardiovascular indices estimated every 2 min from baseline to complete onset of septic shock. For each pig, the indices of baseline windows were averaged to get one value for each index. For each pig, the time trends from the insult (T1) to the development of septic shock (T2) were aligned to the time of insult, which was conventionally set as time zero, allowing responses to be compared across animals. These time series were then smoothed using an exponential moving average with a 10-point window in order to filter out possible artifacts or noises and interpolate missing values in case of short gaps, i.e., less than 10 missing values. Indices from radial pressure recordings were excluded from successive analysis due to the presence of too many long gaps. 23 features were identified as suitable, i.e., gap free and available for each pig, for the successive analyses (Table 1).

Clustering analysis

The clustering analysis was based on the selected time series of indices listed in Table 1. Firstly, they were standardized using the *TimeSeriesScalerMeanVariance* function in Python (*tslearn* library); then, the time series were resampled to a uniform length corresponding to the maximum time required for any animal to reach sepsis

Index	Description	Unit of measure
PPamp	PP amplification from femoral BP	a.u.
SAP_a	Aortic SAP	mmHg
DAP_a	Aortic DAP	mmHg
PP_a	Aortic PP	mmHg
MAP_a	Aortic MAP	mmHg
tau_a	Windkessel time constant τ from aortic BP	s
HD_a	Harmonic distortion index from aortic BP	a.u.
BRS_a	Cardiac baroreflex sensitivity from aortic BP	s/mmHg
FF_a	Feedforward gain from aortic BP	mmHg/s
SSI_a	Systolic shock index HR/SAP from aortic BP	bpm/mmHg
DSI_a	Diastolic shock index HR/DAP from aortic BP	bpm/mmHg
HR	Heart rate	bpm
CO	Cardiac output	L/min
SV	Stroke volume	mL
SAP_f	Femoral SAP	mmHg
DAP_f	Femoral DAP	mmHg
PP_f	Femoral PP	mmHg
MAP_f	Femoral MAP	mmHg
tau_f	Windkessel time constant τ from femoral BP	s
HD_f	Harmonic distortion index from femoral BP	a.u.
BRS_f	Cardiac baroreflex sensitivity from femoral BP	s/mmHg
FF_f	Feedforward gain from femoral BP	mmHg/s
DSI_f	Diastolic shock index HR/DAP from femoral BP	bpm/mmHg

Table 1. List of the cardiovascular indices used in the study. PP: pulse pressure; BP: blood pressure; SAP: systolic arterial pressure; DAP: diastolic arterial pressure; MAP: mean arterial pressure; a.u.: arbitrary units.

onset (about 800 min). Finally, a feature selection was applied in order to optimize the clustering process. To avoid trying all possible combinations, a correlation-based method was used to reduce the number of features³¹. Firstly, the time-lagged cross-correlation (TLCC) was used to measure the redundancy between features and the Inverse Fast Fourier Transform (IFFT) was performed to reduce the computational complexity. Secondly, new correlation-based clustering centroid and stopping criterion were defined to speed up hierarchical clustering. Finally, redundant features were removed using the First Integer Neighbor Clustering Hierarchy (FINCH).

The trend of the indices were clustered by means of a K-mean clustering approach (*TimeSeriesKMeans*, Python, *tslearn* library) with the soft-dynamic time warping (DTW) distance metric (*dtw-python* 1.5.3 library). The optimal number of clusters was determined through the silhouette analysis.

After obtaining the class labels for each animal in the dataset, the cluster means and confidence intervals were calculated for each index. The Wilcoxon rank sum test was used to verify statistical differences in the baseline values between the two clusters.

Shapelet analysis

According to the original definition, a shapelet is a time series subsequence with high predictive power³². In order to obtain a clear interpretation of the clustering results, we used the Shapelet Transform^{33,34}. This method allowed us to identify specific dynamic characteristics of the different classes and select the trends that best explain the cluster decision. Shapelet analysis was performed on the original feature time series before the normalization to extract clinically significant numeric values for each trend curve. The shapelet analysis was performed on each feature, with classification labels extracted from the DTW clustering. The length of the shapelets was set to 180, 240, or 300 min to capture trends rather than local perturbations.

Results

Figure 1 shows the trend of aortic MAP and HR in the overall population. As expected, application of the insult led to a rapid decline in MAP values, with readings dropping below 65 mmHg, thereby inducing a severe hypotensive state. At the same time, a sharp rise in HR was documented in all pigs^{35–37}. Figure 1 also highlights the significant heterogeneity of the pigs' responses to the insult, despite the initial homogeneity of the animal population and the similarity of the insult.

The most significant features identified by the proposed feature selection algorithm, i.e., by measuring feature correlation and removing redundancy based on FINCH, were *PPamp*, *tau_f*, *SAP_a*, and *HD_f*. These indices were subsequently used for the successive clustering analysis.

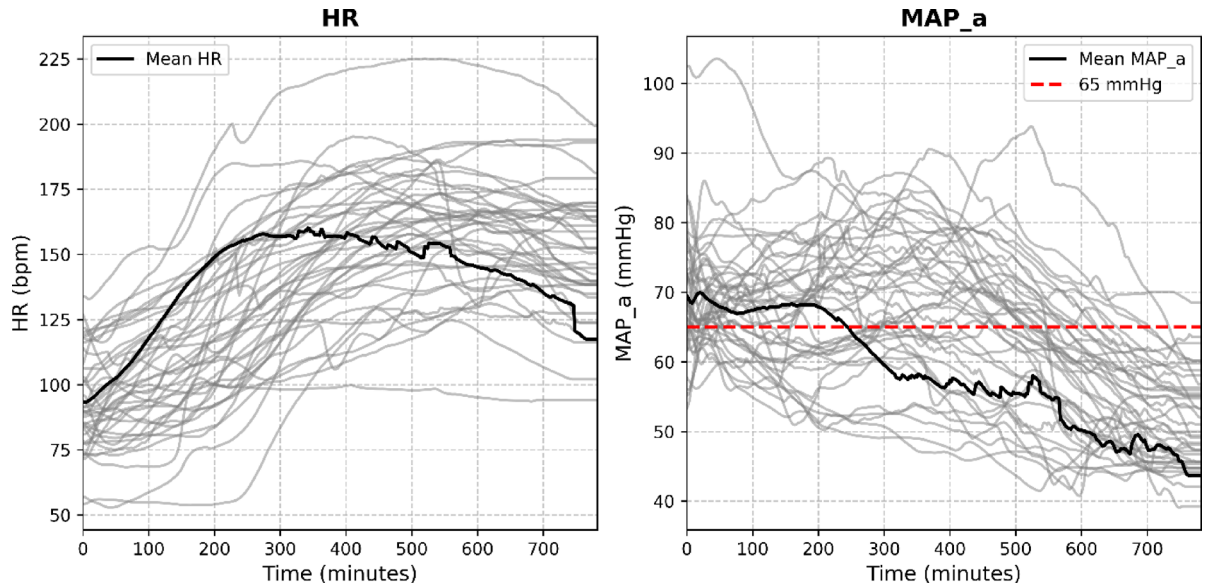


Fig. 1. *Left:* Trends of heart rate (HR) values. *Right:* Trends of mean arterial pressure (MAP) values measured in aorta. Trends are shown from time 0 (T1), corresponding to the moment of feces inoculation, through T2, which marks the development of full septic shock. Trends are stretched to have the same duration (refer to the text for details). Values are shown from insult to shock onset for each pig. Bold black lines represent the population mean. Red dotted line represents the value of arterial blood pressure considered as the clinical threshold for severe hypotension (65 mmHg).

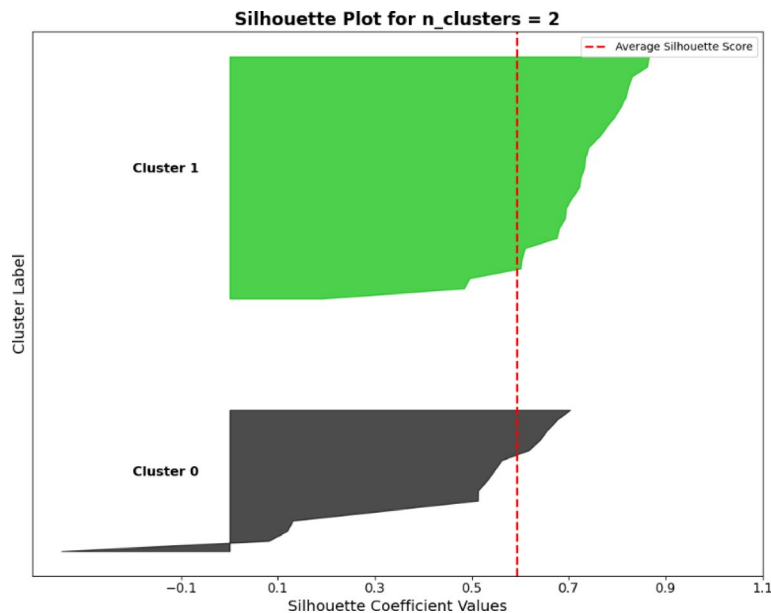


Fig. 2. Silhouette plot with the optimal number of clusters obtained ($n=2$) by considering the 4 features previously identified with the FINCH approach. Silhouette average score = 0.59.

According to the silhouette analysis, the optimal number of clusters obtained was 2, as shown in Fig. 2. The silhouette plot shows a few negative values, indicating that the separation is not perfect. However, a closer inspection of the two histograms reveals that they are clearly separated, with only a few values close to zero.

After obtaining the class labels for each animal, cluster means and confidence intervals have been calculated for each index. Cluster 0 includes $n=15$ pigs, cluster 1 includes $n=25$ pigs. We observed that the time to enter shock was not significantly different between the two clusters (cluster 0: 7.25 ± 2.53 h; cluster 1: 6.39 ± 1.60 h), although the values of the standard deviation highlight a notable intersubject variability. The boxplot distributions of the baseline values for all the indices are shown in supplementary Fig. S1. Statistical analysis revealed that some variables differed significantly between the clusters at baseline. In particular, cluster 0 was characterized

by significantly higher PP and BRS values (for both aortic and femoral arteries), and lower HR, CO, DSI, and SSI values compared to cluster 1. Interestingly, aortic HD was significantly lower in cluster 0 than in cluster 1, whereas the opposite result was found for femoral HD values.

Figure 3 shows the trends of the four most important features according to the FINCH selection algorithm, which were used for the clustering analysis. Other features, i.e., aortic PP, HR, CO, and FF gain, were displayed as well, as they exhibited interesting differences in trends between the two clusters. Supplementary Fig. S2 shows the trends of all the cardiovascular indices used in the study for the two clusters.

SAP_a showed a marked decrease in cluster 0 from the onset of the insult reaching very low systolic pressure values (<65 mmHg). In contrast, animals in cluster 1 exhibited relatively stable pressure levels for a few hours after the insult, followed by a rapid drop, though pressure values remained higher than those of animals in cluster 0. The same trend was observed for aortic DAP and aortic MAP, as well as for femoral ABP (see Fig. S2).

Interestingly, the HD values in cluster 0 exhibited a decreasing trend, akin to the SAP. Conversely, the animals in cluster 1 showed an increasing trend that subsequently stabilized at higher levels. A similar trend was obtained also with HD computed from the aortic ABP signal (see Fig. S2).

The PP amplification index has confirmed the expected inversion of the physiological PP amplification from central to peripheral sites induced by sepsis (Fig. 3). This is indicated by a decrease in the index to values below 1, which occurs in both clusters and before to the overt manifestation of sepsis. It should be noted that the decrease is less pronounced in cluster 1 than in cluster 0.

The Windkessel time constant τ has a decreasing trend, as expected^{8,38}. In cluster 1 the index exhibited a more pronounced drop than in cluster 0 in the first hours after the insult. It subsequently stabilized at a relatively constant level, ultimately ending up with higher values than cluster 0, that, on the contrary, showed a constant decreasing trend.

The trend of the HR and FF gain were similar and differed greatly between the two clusters. Cluster 1 was characterized by higher HR levels and a marked increase in FF gain during the first hours of sepsis development, reaching a plateau. In contrast, cluster 0 showed lower HR levels and a much more gradual increase in FF gain values reaching much lower values than in cluster 1. This is also evident from the higher CO values observed in cluster 1 compared to cluster 0 throughout most of the sepsis progression period; CO values reached similar levels at the end of the development phase principally due to a larger decrease of SV values in cluster 1. This led to a lower CO alongside a higher HR.

Finally, a different trend was also observed in aortic PP values: cluster 1 showed a constant increasing trend, whereas cluster 0 was characterized by an initial rapid decline of PP values followed by a similarly rapid increase up to baseline values.

The results of the shapelet analysis are shown in Fig. 4. They corroborate the clustering analysis by identifying two groups of animals: one with a gradual, monotonic decline in blood pressure, and another with predominantly stable or slightly increasing pressure, mainly visible in the systolic shapelets, followed by a sudden drop. Moreover, shapelet analysis also highlights the opposite trends of HD values in the two clusters, as well as the differences in aortic FF gain values, indeed, some animals showed a rapid increase, while others showed a more gradual rise reaching much lower values.

Figure 5 shows an example of aortic and femoral ABP beats at baseline and after full development of septic shock from two pigs in the two clusters; the computed HD values are also reported.

Discussion

In this study the cardiovascular response of 40 pigs undergoing polymicrobial sepsis induction and septic shock development was continuously monitored using advanced physiological indices derived from aortic and femoral blood pressure signals. The aim was to investigate potential of these indices to improve early detection of sepsis onset and the severity assessment of septic deterioration.

All the animals reached a comparable septic condition according to the main physiological parameters as determined by clinical criteria, such as severe hypotension (MAP < 65 mmHg), compensatory tachycardia^{35–37}, and low CO⁹. Clinical indices as SSI and DSI significantly increased, as expected²⁶. Vascular properties underwent to profound alterations, in particular, aortic AC dramatically dropped, leading to a stiffer arterial system, as already reported in several preclinical and clinical studies^{7,8,38–41}. Moreover, all the animals showed a significant decline of BRS values, highlighting a severe autonomic failure induced by sepsis, consistently with literature evidence¹⁰ (see supplementary Fig. S2). Finally, a PP reversal was found in the overall population occurring well before the clinical manifestations of sepsis signs, indeed, the ratio between femoral and aortic PP decreased to values lower than 1, in agreement with previous experimental studies^{7,8}.

Aside from the common traits observed across the overall population, which generally confirm previous scientific results, our analyses demonstrate great heterogeneity in the cardiovascular response to the insult and indicate that the proposed indices may be able to differentiate these responses.

The unsupervised clustering analysis revealed two primary trend clusters, each exhibiting distinct cardiovascular responses. Specifically, animals in cluster 1 appeared to compensate for the reduced perfusion and CO caused by the inflammatory insult through an elevated HR. This initially helped maintain stable blood pressure; however, hypotension developed successively (Fig. 3). In contrast, animals in cluster 0 exhibited a progressive decline in blood pressure, reaching lower levels than those in cluster 1, accompanied by reduced CO and HR. These animals appear unable to adequately compensate for the inflammatory stress, resulting in a faster deterioration of physiological parameters.

Cluster 1 is characterized by an increased FF gain, that could be related to the lower values of AC assessed in these animals. The decreased AC inevitably limits the Windkessel effect of the large arteries²⁹, as a consequence, the blood flow could arrive at peripheral districts with a higher pulsatility; this, combined with the vasoplegic state typical of septic shock, could result in amplified oscillations in ABP induced by an elevated HR.

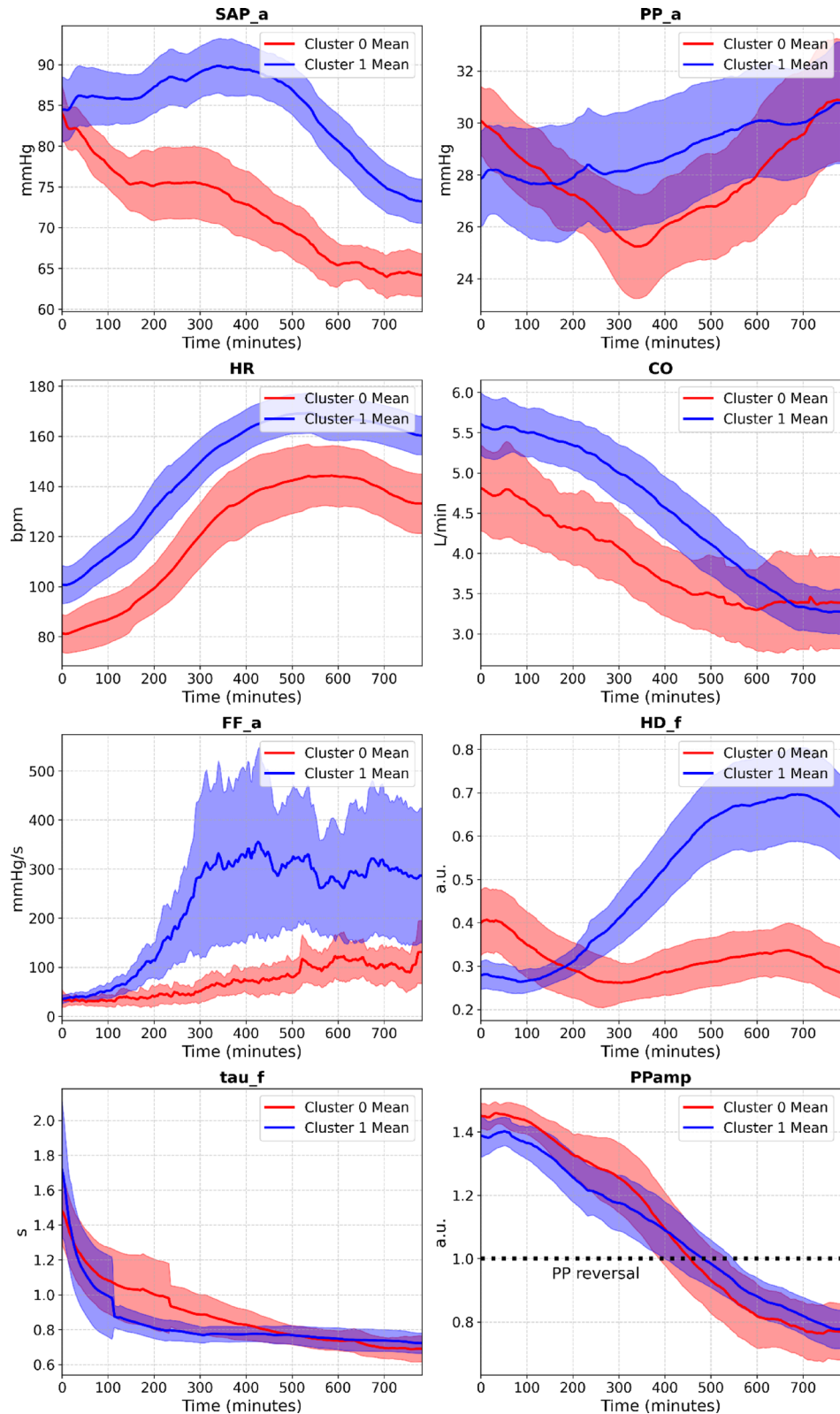


Fig. 3. Trends in eight cardiovascular variables in the two clusters. Trends are shown from time 0 (T1), corresponding to the moment of feces inoculation, through T2, which marks the development of full septic shock. The trends are stretched to have the same duration (refer to the text for details). The lines represent the cluster mean and the shadow areas represent the 95% confidence interval. Cluster 0 is marked in red and cluster 1 in blue. SAP_a: aortic systolic blood pressure; PP_a: aortic pulse pressure; HR: heart rate; CO: cardiac output; FF_a: feedforward gain computed from aortic blood pressure signal; HD_f: harmonic distortion estimated from femoral blood pressure; tau_f: Windkessel time constant τ from femoral blood pressure; PPamp_f: pulse pressure amplification estimated with femoral blood pressure.

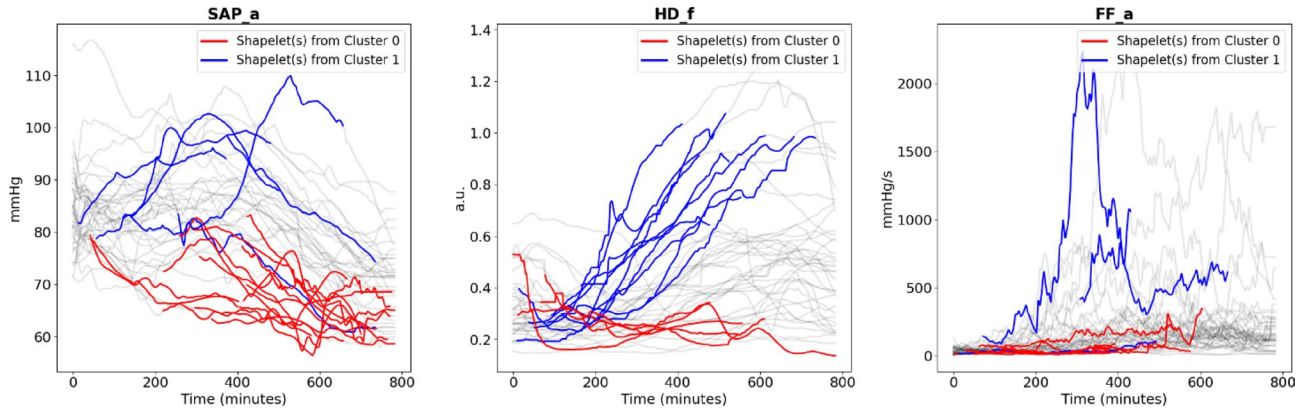


Fig. 4. Results from the shapelet analysis highlighting the most discriminative temporal patterns across variables. Red and blue lines represent shapelets from cluster 0 and cluster 1, respectively, overlaid on all individual trajectories (gray). Trends are shown from time 0 (T1), corresponding to the moment of feces inoculation, through T2, which marks the development of full septic shock. SAP_a: aortic systolic blood pressure; HD_f: harmonic distortion estimated from femoral blood pressure; FF_a: feedforward gain computed from aortic blood pressure signal.

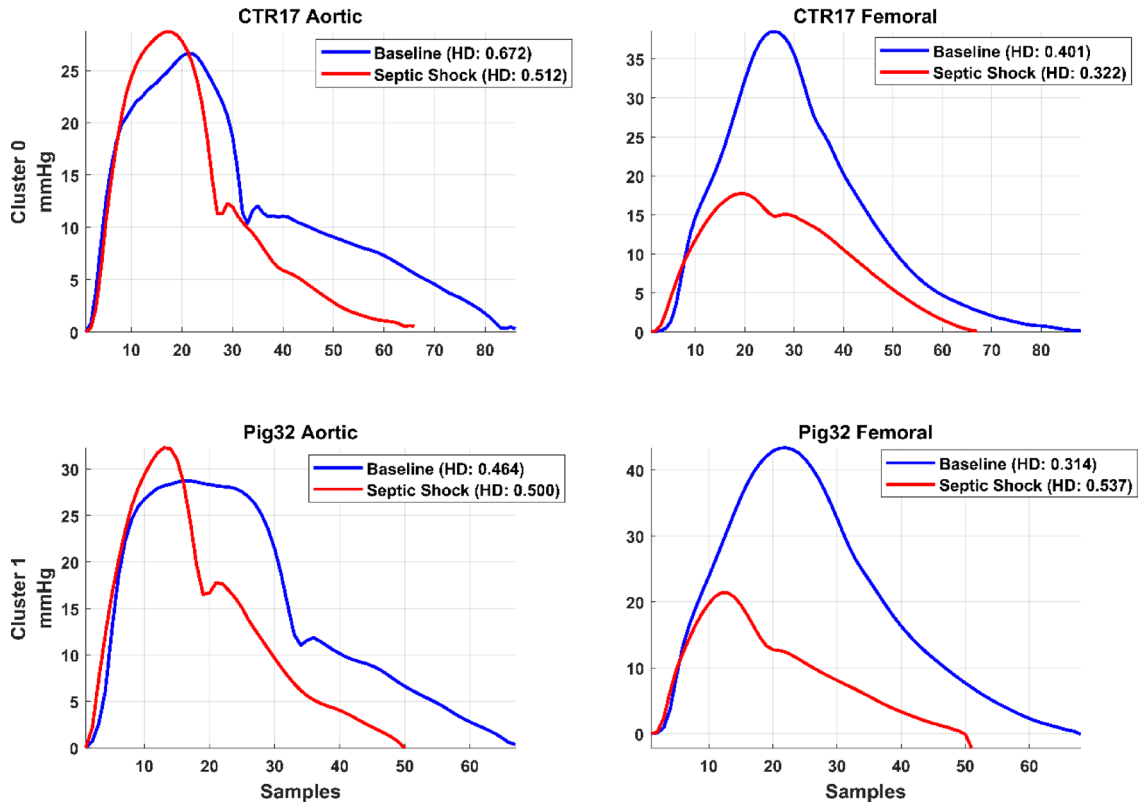


Fig. 5. Representative waveform templates from two experimental animals: CTR17 (Cluster 0) and Pig32 (Cluster 1). The aortic and femoral pressure waveforms are shown at baseline (blue) and in septic shock (red) condition. HD denotes harmonic distortion and reflects waveform complexity. Cluster 0 exhibits decreases waveform complexity after septic shock onset, whereas Cluster 1 preserves or increases it.

This phenomenon may also be related to the increase in HD values in cluster 1. HD is a quantitative metric of pulse wave complexity, reflecting the number of reflected waves. A waveform with a lower degree of complexity should exhibit a lower HD index⁴². As previously observed in other experiments⁴², cluster 0 demonstrates a consistent trend where sepsis development induces a decrease in HD index and this is associated with an overall decrease in wave reflections, producing a simpler arterial waveform, like the bell-shaped type B waveform. Cluster 1 shows a different trend, i.e., an increase in HD index (see Fig. 3). This could also be affected by the

HR, that is known to impact reflection phenomena^{43,44}, likely due to alterations in the timing of the reflected pressure wave produced by changes in the systolic duration. Figure 5 clearly illustrate the different morphological characteristics of the ABP waveform at baseline and after septic shock development in the two clusters, consistent with the HD index values. In cluster 0 the HD index decreased as both aortic and femoral ABP waveforms became simpler under septic shock conditions, showing a smoother and more bell-shaped profile without a visible systolic inflection. Conversely, in cluster 1, the ABP waveform became more complex under septic shock conditions, with the systolic inflection still apparent and the dicrotic notch in the femoral trace becoming more pronounced compared to baseline condition.

Finally, the shapelet analysis further corroborated the results of the clustering analysis, with the most significant trends revealing distinct temporal patterns in each cluster, characterized by markedly different evolutions of SAP, HD, and FF gain values.

The significant differences between the two clusters observed at baseline are mostly related to indices related to autonomic, e.g., BRS, and vascular properties, e.g., HD, PP, TPR, tau. Standard clinical variables, such as MAP, were homogeneous in the cohort before sepsis induction. This result has two important implications. First, it suggests that the same experimental procedure may not elicit identical cardiovascular responses across animals, even when global hemodynamic indices appear homogeneous. Second, this initial heterogeneity in cardiovascular function among the pigs may have influenced their differential responses to the septic insult. Consequently, the proposed indices could prove useful not only for assessing septic deterioration, but also for prior risk stratification.

The clinical management of septic patients could be improved by incorporating the proposed unconventional vascular indices into bedside monitoring systems. This would help clinicians to anticipate severe deterioration, intervene before overt clinical manifestations of sepsis occur, and tailor the therapy on the basis of the observed trends. Because these indices can be readily computed from routinely acquired arterial line signals, they can be readily translated into clinical practice.

Conclusion

In the present study we investigated the cardiovascular response to sepsis over time, using both standard hemodynamic parameters, such as MAP, HR, CO, and novel ABP waveform-derived indices that may reflect vascular properties, such as PP amplification, Windkessel time constant, and HD. Sepsis is known to cause significant vascular dysfunction; therefore, these specific indices could aid clinicians in the early detection and assessment of sepsis severity, potentially enabling more timely and personalized treatment strategies for critically ill patients. Our findings strengthen the potential of these indices as they report on two different trends from the insult up to the full development of septic shock, in an apparently homogeneous cohort according to the clinical guidelines. Indeed, the insult, endpoints and interventions were standardized based on criteria commonly employed in sepsis clinical trials. In particular, our results suggests that the cardiac response may play a greater role in one group of animals than in the other in order to compensate a larger vascular alteration.

Limitations and further developments

The main limitation of this study is the exclusive reliance on preclinical data collected from a homogeneous population of healthy young swine. Future investigations should address the broader heterogeneity of the clinical population characterized by a large variability in age, comorbidities, and sepsis severity. Moreover, further research is necessary to investigate the potential relationship between these trends and the severity of inflammation measured by inflammatory markers (e.g., cytokines, endothelin, etc.) or other clinical outcomes, as well as to verify possible associations between the trends observed before sepsis onset and the administered therapy used during resuscitation so to tailor a personalized resuscitation strategy.

Data availability

Data available upon request.

Received: 20 October 2025; Accepted: 27 January 2026

Published online: 02 February 2026

References

- Rudd, K. E. et al. Global, regional, and National sepsis incidence and mortality, 1990–2017: analysis for the global burden of disease study. *Lancet* **395**, 200–211 (2020).
- Iwashyna, T. J., Ely, E. W., Smith, D. M. & Langa, K. M. Long-term cognitive impairment and functional disability among survivors of severe sepsis. *JAMA* **304**, 1787–1794 (2010).
- van der Slikke, E. C., An, A. Y., Hancock, R. E. W. & Bouma, H. R. Exploring the pathophysiology of post-sepsis syndrome to identify therapeutic opportunities. *EBioMedicine* **61**, 103044 (2020).
- Goodwin, A. J., Rice, D. A., Simpson, K. N. & Ford, D. W. Frequency, cost, and risk factors of readmissions among severe sepsis survivors. *Crit. Care Med.* **43**, 738–746 (2015).
- Rawal, G., Yadav, S. & Kumar, R. Post-intensive care syndrome: an overview. *J. Transl. Int. Med.* **5**, 90–92 (2017).
- Kosyakovskiy, L. B. et al. Association between sepsis survivorship and long-term cardiovascular outcomes in adults: a systematic review and meta-analysis. *Intensive Care Med.* **47**, 931–942 (2021).
- Hatib, F., Jansen, J. R. C. & Pinsky, M. R. Peripheral vascular decoupling in Porcine endotoxemic shock. *J. Appl. Physiol.* **111**, 853–860 (2011).
- Carrara, M., Herpain, A., Baselli, G. & Ferrario, M. Vascular decoupling in septic shock: the combined role of autonomic nervous System, arterial Stiffness, and peripheral vascular tone. *Front. Physiol.* **11**, 1–13 (2020).
- Singer, M. et al. The third international consensus definitions for sepsis and septic shock (sepsis-3). *JAMA - J. Am. Med. Association.* **315**, 801–810 (2016).

10. Carrara, M., Ferrario, M., Pinto, B. B. & Herpain, A. The autonomic nervous system in septic shock and its role as a future therapeutic target: a narrative review. *Ann. Intensive Care* **11**, (2021).
11. Guberti, D., Ferrario, M., Liu, S., Jakob, S. M. & Carrara, M. Wave separation analysis to assess cardiovascular alterations induced by sepsis. *IEEE Trans. Biomed. Eng.* **71**, 1719–1731 (2024).
12. Campitelli, R. et al. Pulse wave analysis as a tool for the evaluation of resuscitation therapy in septic shock. *Physiol. Meas.* **44**, 105002 (2023).
13. Hyland, S. L. et al. Early prediction of circulatory failure in the intensive care unit using machine learning. *Nat. Med.* **26**, 364–373 (2020).
14. Hatib, F. et al. Machine-learning algorithm to predict hypotension based on High-fidelity arterial pressure waveform analysis. *Anesthesiology* **129**, 663–674 (2018).
15. Chiew, C. J. et al. Heart rate variability based machine learning models for risk prediction of suspected sepsis patients in the emergency department. *Medicine* **98**, e14197 (2019).
16. Mollura, M., Lehman, L. W. H., Mark, R. G. & Barbieri, R. A novel artificial intelligence based intensive care unit monitoring system: using physiological waveforms to identify sepsis. *Philos. Trans. Royal Soc. A Math. Phys. Eng. Sci.* **379**, (2021).
17. Pasquale, M. et al. Hemorrhage prediction models in surgical intensive care: bedside monitoring data adds information to lab values. *IEEE J. Biomed. Health Inf.* **21**, 1703–1710 (2017).
18. Moorman, J. R. et al. Cardiovascular oscillations at the bedside: early diagnosis of neonatal sepsis using heart rate characteristics monitoring. *Physiol. Meas.* **32**, 1821–1832 (2011).
19. Carrara, M., Niccolo, A., Herpain, A. & Ferrario, M. Reducing tachycardia in septic shock patients: do esmolol and ivabradine have a chronotropic effect only? In *2020 42nd Annual International Conference of the IEEE Engineering in Medicine & Biology Society (EMBC)* 382–385. <https://doi.org/10.1109/EMBC44109.2020.9176309> (IEEE, 2020).
20. Garcia, B. et al. Myocardial effects of angiotensin II compared to norepinephrine in an animal model of septic shock. *Crit. Care.* **26**, 281 (2022).
21. Garcia, B. et al. Inhibition of Circulating dipeptidyl-peptidase 3 by Procizumab in experimental septic shock reduces catecholamine exposure and myocardial injury. *Intensive Care Med. Exp.* **12**, 53 (2024).
22. Percie du Sert. The ARRIVE guidelines 2.0: updated guidelines for reporting animal research. *PLoS Biol.* **18**, e3000410 (2020).
23. Osuchowski, M. F. et al. Minimum quality threshold in Pre-Clinical sepsis studies (MQTiPSS): an international expert consensus initiative for improvement of animal modeling in sepsis. *Shock* **50**, 377–380 (2018).
24. Zong, W., Heldt, T., Moody, G. B. & Mark, R. G. An open-source algorithm to detect onset of arterial blood pressure pulses. *Computers Cardiol.* **2003**, 259–262. <https://doi.org/10.1109/CIC.2003.1291140> (2003).
25. Sun, J. X. et al. A signal abnormality index for arterial blood pressure waveforms. *Med. Biol. Eng. Comput.* **42**, 698–706 (2004).
26. Ospina-Tascón, G. A., García-Gallardo, G. & Orozco, N. Using the diastolic shock index to determine when to promptly administer vasopressors in patients with septic shock. *Clin. Exp. Emerg. Med.* **9**, 367–369 (2022).
27. Barbieri, R., Parati, G. & Saul, J. P. Closed- versus open-loop assessment of heart rate baroreflex. *IEEE Eng. Med. Biol. Mag.* **20**, 33–42 (2001).
28. Milkovich, N., Gkousioudi, A., Seta, F., Suki, B. & Zhang, Y. Harmonic distortion of blood pressure waveform as a measure of arterial stiffness. *Front. Bioeng. Biotechnol.* **10**, 1–11 (2022).
29. Westerhof, N., Lankhaar, J. W. & Westerhof, B. E. The arterial Windkessel. *Med. Biol. Eng. Comput.* **47**, 131–141 (2009).
30. Lu, Z. & Mukkamala, R. Continuous cardiac output monitoring in humans by invasive and noninvasive peripheral blood pressure waveform analysis. *J. Appl. Physiol.* **101**, 598–608 (2006).
31. Wang, L., Liu, W. & Chu, Z. Unsupervised feature selection for multivariate time series based on improved FINCH. In *Proceedings of the 2023 6th International Conference on Machine Learning and Natural Language Processing* 111–115. <https://doi.org/10.1145/3639479.3639503> (ACM, 2023).
32. Bock, C. et al. Association mapping in biomedical time series via statistically significant shapelet mining. *Bioinformatics* **34**, i438–i446 (2018).
33. Lines, J., Davis, L. M., Hills, J. & Bagnall, A. A shapelet transform for time series classification. In *Proceedings of the 18th ACM SIGKDD International Conference on Knowledge Discovery and Data Mining* 289–297. <https://doi.org/10.1145/2339530.2339579> (ACM, 2012).
34. Hills, J., Lines, J., Baranauskas, E., Mapp, J. & Bagnall, A. Classification of time series by shapelet transformation. *Data Min. Knowl. Discov.* **28**, 851–881 (2014).
35. Morelli, A., Egidio, A. D. & Passariello, M. Tachycardia in septic shock: pathophysiological implications and pharmacological treatment. In *Annual Update in Intensive Care and Emergency Medicine* Vincent JL (eds) **2015** (Springer, 2015).
36. Rudiger, A. & Singer, M. The heart in sepsis: from basic mechanisms to clinical management. *Curr. Vasc Pharmacol.* **11**, 187–195 (2013).
37. Merx, M. W. & Weber, C. Sepsis and the heart. *Circulation* **116**, 793–802 (2007).
38. Carrara, M. et al. Autonomic and circulatory alterations persist despite adequate resuscitation in a 5-day sepsis swine experiment. *Sci. Rep.* **12**(1), 19279. <https://doi.org/10.1038/s41598-022-23516-y> (2022).
39. Vlachopoulos, C. et al. Acute systemic inflammation increases arterial stiffness and decreases wave reflections in healthy individuals. *Circulation* **112**, 2193–2200 (2005).
40. Leclerc, J. et al. A single endotoxin injection in the rabbit causes prolonged blood vessel dysfunction and a procoagulant state. *Crit. Care Med.* **28**, 3672–3678 (2000).
41. Kazune, S., Grabovskis, A., Cescon, C., Strike, E. & Vanags, I. Association between increased arterial stiffness and clinical outcomes in patients with early sepsis: a prospective observational cohort study. *Intensive Care Med. Exp.* **7**, (2019).
42. Guberti, D., Ferrario, M., Liu, S., Jakob, S. M. & Carrara, M. Wave separation analysis to assess cardiovascular alterations induced by sepsis. *IEEE Trans. Biomed. Eng.* **1–14** <https://doi.org/10.1109/TBME.2023.3349104> (2024).
43. Mthembu, N. et al. Increased backward wave pressures rather than flow explain Age-Dependent heart rate effects on Central, but not peripheral arterial pressure. *Hypertension* **79**, 435–446 (2022).
44. Wilkinson, I. B. et al. The influence of heart rate on augmentation index and central arterial pressure in humans. *J. Physiol.* **525**, 263–270 (2000).

Acknowledgements

The authors want to acknowledge all investigators from the Experimental Laboratory of Intensive Care at the Universite Libre de Bruxelles: Antoine Herpain, Fuhong Su, Bruno Garcia, Fabio Silvio Taccone and Jacques Creteur.

Author contributions

IV performed the analyses and provided edits to the manuscript, MF and MC conceived the study, provided supervision to the project and drafted the manuscript.

Declarations

Competing interests

The authors declare no competing interests.

Additional information

Supplementary Information The online version contains supplementary material available at <https://doi.org/10.1038/s41598-026-37885-1>.

Correspondence and requests for materials should be addressed to M.C.

Reprints and permissions information is available at www.nature.com/reprints.

Publisher's note Springer Nature remains neutral with regard to jurisdictional claims in published maps and institutional affiliations.

Open Access This article is licensed under a Creative Commons Attribution-NonCommercial-NoDerivatives 4.0 International License, which permits any non-commercial use, sharing, distribution and reproduction in any medium or format, as long as you give appropriate credit to the original author(s) and the source, provide a link to the Creative Commons licence, and indicate if you modified the licensed material. You do not have permission under this licence to share adapted material derived from this article or parts of it. The images or other third party material in this article are included in the article's Creative Commons licence, unless indicated otherwise in a credit line to the material. If material is not included in the article's Creative Commons licence and your intended use is not permitted by statutory regulation or exceeds the permitted use, you will need to obtain permission directly from the copyright holder. To view a copy of this licence, visit <http://creativecommons.org/licenses/by-nc-nd/4.0/>.

© The Author(s) 2026